Am J Physiol Cell Physiol 317: C326–C338, 2019.
First published May 8, 2019; doi:10.1152/ajpcell.00128.2018.

RESEARCH ARTICLE

Integrated proteomics and metabolomics analysis reveals differential lipid metabolism in human umbilical vein endothelial cells under high and low shear stress

Gabriela Venturini,[1] Pamella Araujo Malagrino,[1] Kallyandra Padilha,[1] Leonardo Yuji Tanaka,[2] Francisco Rafael Laurindo,[2] Rafael Dariolli,[1] Valdemir Melechco Carvalho,[3] Karina Helena Morais Cardozo,[3] Jose Eduardo Krieger,[1] and Alexandre da Costa Pereira[1]

[1]*Laboratory of Genetics and Molecular Cardiology, Heart Institute (InCor), Faculdade de Medicina FMUSP, Universidade de Sao Paulo, Sao Paulo, Brazil;* [2]*Vascular Biology Laboratory, Heart Institute (InCor), Faculdade de Medicina FMUSP, Universidade de Sao Paulo, Sao Paulo, Brazil; and* [3]*Fleury Group, Sao Paulo, Brazil*

Submitted 4 April 2018; accepted in final form 30 April 2019

Venturini G, Malagrino PA, Padilha K, Tanaka LY, Laurindo FR, Dariolli R, Carvalho VM, Cardozo KH, Krieger JE, Pereira AC. Integrated proteomics and metabolomics analysis reveals differential lipid metabolism in human umbilical vein endothelial cells under high and low shear stress. *Am J Physiol Cell Physiol* 317: C326–C338, 2019. First published May 8, 2019; doi:10.1152/ajpcell.00128.2018.—Atherosclerotic plaque development is closely associated with the hemodynamic forces applied to endothelial cells (ECs). Among these, shear stress (SS) plays a key role in disease development since changes in flow intensity and direction could stimulate an atheroprone or atheroprotective phenotype. ECs under low or oscillatory SS (LSS) show upregulation of inflammatory, adhesion, and cellular permeability molecules. On the contrary, cells under high or laminar SS (HSS) increase their expression of protective and anti-inflammatory factors. The mechanism behind SS regulation of an atheroprotective phenotype is not completely elucidated. Here we used proteomics and metabolomics to better understand the changes in endothelial cells (human umbilical vein endothelial cells) under in vitro LSS and HSS that promote an atheroprone or atheroprotective profile and how these modifications can be connected to atherosclerosis development. Our data showed that lipid metabolism, in special cholesterol metabolism, was downregulated in cells under LSS. The low-density lipoprotein receptor (LDLR) showed significant alterations both at the quantitative expression level as well as regarding posttranslational modifications. Under LSS, LDLR was seen at lower concentrations and with a different glycosylation profile. Finally, modulating LDLR with atorvastatin led to the recapitulation of a HSS metabolic phenotype in EC under LSS. Altogether, our data suggest that there is significant modulation of lipid metabolism in endothelial cells under different SS intensities and that this could contribute to the atheroprone phenotype of LSS. Statin treatment was able to partially recover the protective profile of these cells.

endothelial cell; lipids and lipoprotein metabolism; shear stress

INTRODUCTION

Endothelial cells (ECs) are specialized cells located between the blood flow and the vascular wall. They act in both structural and signaling realms of vascular biology. As a structural actor, ECs form a nonthrombogenic and selective barrier between blood and smooth muscle cells, allowing the selective permeability of circulating cells and macromolecules. ECs are also involved in many other functions such as cell migration, vessel remodeling, physiological control of the vascular lumen, maintenance of anticoagulant properties, secretion of factors, biomolecule metabolism, and even smooth muscle cell contractility (12, 17, 70).

All those functions are strictly modulated either by the biochemical coupling of cytokines, growth factors, and lipoproteins or by hemodynamic forces, to which ECs are continuously and directly exposed. These hemodynamic forces act at the cellular surface triggering mechanotransduction signals that modulate the activation of many pathways (47) both by gene expression and posttranscriptional mechanisms.

One of the main mechanical stimuli is shear stress (SS), a frictional force of blood flow that acts tangential to the EC apical surface and contributes to vascular homeostasis (19, 47). Molecules located in the apical surface, such as the glycocalyx (53), several different receptors (5, 73), ion channels (32), and membrane lipids (77), are highly sensitive to this stimuli. Other molecules that are not located in the surface are also SS targets, such as cell junction complex (30, 69), extracellular matrix (79), and structural proteins (29, 33). These mechanical sensors have the ability to convert physical stress to biochemical signals through adaptor proteins resulting in the activation of signaling pathways [for example, those downstream of the Krüppel-like factor (KLF) family (22, 45, 49, 56, 59) and NF-κB (43, 73)].

The vascular tree does not have a uniform SS distribution. This results in areas with laminar SS and regions with low or oscillatory flow (64). Atherosclerotic lesions preferably develop in regions where the flow is not laminar and uniform [i.e., low shear stress (LSS)] such as bifurcations and curvatures (11). Genomic and proteomic studies have shown that endothelial genes are regulated in these regions, leading to the expression of proteins that promote predisposition to atherosclerotic plaque formation (74). In areas of LSS there is an upregulation of proinflammatory cytokines and targets of the NF-κB pathway (1, 61, 67), a higher oxidative stress (1, 20, 31, 34), an increase in adhesion molecules expression (13, 14) and

Address for reprint requests and other correspondence: G. Venturini. Av Dr Enéas de Carvalho Aguiar, 44 - 10th floor, 05403-000, São Paulo, SP, Brazil (e-mail: venturini.gabriela@gmail.com).

vascular permeability to molecules such as LDL (30, 68), and changes in glycolytic metabolism modulated by hypoxia-inducible factor-1α (23). On the other hand, ECs under laminar and uniform flow show a protective gene expression pattern, with upregulation of anti-inflammatory molecules, and maintenance of the permeability barrier and the redox state.

Despite the extensive literature associating inflammation, oxidative stress, and upregulation of adhesion molecules with SS intensity, there is little evidence on the relative importance of cellular lipid metabolism and lipid content regarding EC flow-dependent modulations. Membrane lipid content is important for cellular homeostasis since these macromolecules are involved in several cellular processes such as integrin activation, actin polymerization, endocytosis, and caveola formation. Lipid rafts, sites where many signaling proteins are located, such as endothelial nitric oxide synthase, G proteins, caveolin, and glycosyl-phosphatidylinositol-anchored proteins (62, 63), show a fine tune regulation regarding the classes and relative proportion of lipids that constitute them. Changing the type of membrane lipid constitution can impair the lipid raft structure leading to activation or inhibition of pathways (26) such as ERK phosphorylation, VCAM and ICAM upregulation, and cytokine expression. In addition, the type of lipid that constitutes the cells can interfere in cellular rigidity, number of focal adhesion, and endothelial permeability.

Here we integrated stable isotope labeling by amino acids (SILAC) proteomics and metabolomics to understand additional pathways that are modulated in ECs under atheroprone (LSS) and atheroprotective (HSS) flow. Combing these two techniques we show that lipid metabolism is downregulated in cells under LSS accompanied by a significant difference in the amount and glycosylation of low-density lipoprotein receptor (LDLR). Modulating LDLR with statin treatment in LSS, we could recover part of the atheroprotective phenotype of ECs seem in HSS.

MATERIALS AND METHODS

Cell culture. Human umbilical vein endothelial cells (HUVECs; no. C0035C; Thermo Scientific) from a single newborn male donor were cultivated in endothelial basal medium (EBM-2; no. CC-3156; Lonza) supplemented with EGM-2 growth factors (no. CC-3162; Lonza) in an incubator at 37°C with 5% of CO_2. For SILAC experiments, cells were cultivated in special medium as described below.

SILAC labeling. For isotopic labeling, cells were cultivated in medium containing heavy lysine and arginine following the protocol of Ong and collaborators (7, 37, 51). Briefly, HUVECs were cultivated in DMEM-F-12 SILAC (no. A2494301; Thermo Scientific) supplemented with hEGF, hydrocortisone, GA-1000 (gentamicin, amphotericin-B), dialyzed FBS, VEGF, hFGF-B, R3, IGF-1, ascorbic acid, heparin, arginine 13C6, 15N4 (no. 608033, Sigma-Aldrich), lysine 13C6 15N2 (no. 608041; Sigma-Aldrich), and glutamine (for heavy condition) or the same medium but changing the heavy arginine and lysine by regular arginine and lysine (light condition). Cells were grown in heavy medium until 90% of proteins were labeled (confirmed by mass spectrometry), approximately five passages. We also added proline in the medium to avoid the convention of arginine to proline, which can happen when arginine is highly concentrated in the cell culture medium. After isotopic labeling, heavy cells were submitted to 15 or 5 dyn/cm^2 intercalated to avoid bias or no-labeled contaminants.

Shear stress. HUVECs were kept in starving conditions without supplement during 16 h before SS. After starving, cells were washed and submitted to high shear stress (HSS = 15 dyn/cm^2) and low shear stress (LSS = 5 dyn/cm^2) for 24 h in a cone plate system (6). After 24 h, media were collected for nitrite and nitrate measurement and cells were harvested for proteomics and metabolomics analysis. Each sample is a pool of three plates submitted to in vitro SS cone plate system at the same time, resulting in five samples of LSS and five samples of HSS.

Protein extraction. Proteins were extracted with 8 M urea, 50 mM Tris·HCl pH 8.0, 150 mM NaCl, 1 mM EDTA, and protease/phosphatase cocktail inhibitors (nos. P8340, P2850, and P0044; Sigma-Aldrich). The extract was centrifuged for 15 min at 15,800 *g*, and supernatants were frozen for proteomics analysis. Proteins were quantified by bicinchoninic acid method (no. 23225; Thermo Scientific), and the proteins from HSS and LSS (one condition heavy labeled and the other light labeled) were mixed in the rate 1:1 (heavy/light).

Protein digestion. Proteins (100 μg) were reduced using 10 mM DTT (no. V3151; Promega) during 30 min at 37°C and alkylated using 50 mM iodoacetamide (no. I6125; Sigma-Aldrich) 30 min at room temperature. Trypsin (no. V5111; Promega) was added to the protein lysates at a ratio of 1:50 (wt/wt) for digestion at 37°C for 16 h. Peptides were desalted using Sep-Pak C18 cartridges (no. WAT023590; Waters) and lyophilized.

Mass spectrometry analysis. Peptides were separated by nanoflow LC coupled online to a quadrupole Orbitrap mass spectrometer with a nanoelectrospray ion source. The peptides were loaded on an in house-made biphasic C18/SCX MudPIT column. For optimal separation, an 11-step salt pulse gradient (25, 50, 75, 100, 150, 200, 250, 300, 500, and 750 mM and 1 M ammonium acetate) was performed with 120-min run for each fraction. Following each salt pulse, peptides were gradient-eluted from the reverse analytical column at a flow rate of 500 nl/min. A data-dependent "top 10" method was selected for fragmentation. For survey scans (mass range, 300–1,750 Th), the target value was 3,000,000 with a maximum injection time of 20 ms and a resolution of 70,000 at *m/z* 400. An isolation window of 1.6 Th was used for higher energy collisional dissociation with normalized collision energies of 25 eV. For MS/MS scans, the target ion value was set to 1,000,000 with a maximum injection time of 60 ms, a resolution of 17,500 at *m/z* 400, and dynamic exclusion of 25 s.

Data processing. We used the MaxQuant software environment (version 1.4.3.9) to analyze MS raw data. The MS/MS spectra were searched against the Swissprot database (jun/2016) using the Andromeda search engine incorporated in the MaxQuant framework. Variable modifications Lys8 and Arg10, protein NH_2-terminal acetylation, and oxidized methionine were included. Carbamidomethylated cysteine was included as a fixed modification. Full trypsin specificity was selected as digestion mode, and the maximum missed cleavages was set to 2. Peptides with lengths of a minimum of seven amino acids were considered, with both the peptide and protein false discovery rate set to 1%. Precursor mass tolerance was set to 20 ppm for the first search and 4.5 ppm for the main search. Product ions were searched with a mass tolerance of 20 ppm. Normalized ratio quantification was performed using quantities of unique and razor peptides and a minimum of two peptides was required. Protein groups marked as contaminant, reverse, or "identified by site only" in MaxQuant results were discarded. For SILAC protein ratios, a minimum of one unique peptide and a minimum ratio count of two were required. All reported protein groups were identified with two or more distinct peptides, and were quantified with two or more ratio counts. The mass spectrometry proteomics data have been deposited to the ProteomeXchange Consortium via the PRIDE (71) partner repository with the data set identifier PXD011040.

Differential proteins. For identification of differential proteins, the normalized HSS/LSS ratios were log2 transformed and a significance B test (58) was applied for each sample using Perseus software (15). For follow-up analysis, we used proteins that showed a $P < 0.05$ in at least two samples. Hierarchic cluster was used with log2 of ratios using the Ward D algorithm and Euclidian distance. Analyses were performed in MetaboAnalyst.

Proteins with HSS/LSS ratio equal or higher than 1.25 were considered upregulated in HSS, and proteins with HSS/LSS ratio equal or lower than 0.8 were considered upregulated in LSS.

Statin treatment and SS. HUVECs were treated with 5 μM atorvastatin (no. PZ001; Sigma-Aldrich) or 5 μM atorvastatin plus 10 mM of nitro-L-arginine methyl ester (no. N5751; Sigma-Aldrich) during 72 h diluted in EGM-2 medium. After treatment, cells were submitted to 5 dyn/cm^2 for 24 h. Controls were treated with DMSO. Each sample is a pool of three plates submitted to in vitro SS cone plate system at the same time, resulting in six samples of each condition.

Metabolite extraction and derivatization. After SS, cells were washed with cold PBS and metabolites were extracted with 1 ml of Acetonitrile (no. 34967; Sigma-Aldrich):2-propanol (no. 34965; Sigma-Aldrich):UltraPure water (3:3:2 vol/vol) cold and degassed solution. The solution containing the metabolites was centrifuged for 5 min at 15,800 *g* and 0°C. The supernatant was transferred to a new tube and dried 16 h in SpeedVac. The pellet was washed with 1 ml acetronitrile:UltraPure water (1:1 vol/vol) cold solution and centrifuged for 5 min at 115,800 *g* and 0°C, and the supernatant was transferred to a new tube, spiked with 5 μl of the internal standard myristic acid d27 3 mg/ml (no. 366889; Sigma-Aldrich), and dried 16 h in SpeedVac. Pellets were stored in desiccator at 4°C until analysis.

For derivatization, the pellet was suspended in 20 μl methoxyamine (no. 226904; Sigma-Aldrich) in pyridine (no. 270407; Sigma-Aldrich) solution (40 mg/ml), 3 μl of fatty acid methyl ester (FAME; no. 18919; Sigma-Aldrich) were added, and the mixture was vortexed for 3 min. This methoximation reaction was performed at room temperature for 16 h, followed by trimethylsilylation for 1 h addition of 80 μl *N*-methyl-*N*-trimethylsilyltrifluoroacetamine (MSTFA; no. 69479; Sigma-Aldrich) with 1% trimethylchlorosilane (TCMS; no. 89585; Sigma-Aldrich). After derivatization, 1 μl of this derivative was used for gas chromatography mass spectrometry (GC/MS) analysis.

Gas chromatography and mass spectrometry analysis. One microliter of each sample was injected into an Agilent 7890B GC system operated in splitless mode. A DB5-MS + 10 m Duraguard capillary column (no. 122-5532G; Agilent) within which helium carrier gas flowed at a rate of 1.1 ml/min was applied for metabolite separation. The injector temperature was set at 250°C. The column temperature was held at 60°C for 1 min and then increased to 310°C at a rate of 10°C/min during 37 min. The column effluent was introduced into the ion source of an Agilent 5977A mass selective detector. The detector operated in the electron impact ionization mode (70 eV) and mass spectra were recorded after a solvent delay of 6.5 min with 2.9 scans per second, starting at mass 50 and ending at mass 550, with a step size of 0.1 *m/z*. The MS quadrupole temperature was set at 180°C, and the ion source temperature was set at 280°C. Each sample was analyzed in three technical replicates.

Metabolomic data analysis and statistical methods. Data were deconvoluted with retention time (RT) size window of 75 and 100, signal-to-noise threshold of 1, and extraction window *m/z* delta of 0.3 AMU on left and 0.7 on right. Identification of compounds was made comparing the mass spectra and retention time (RT) of all detected compounds with the Agilent Fiehn GC/MS Metabolomics RTL Library (version A.02.02) containing the spectra profile and RT of 1,447 compounds. RT penalty function was set as Trapezoidal in RT range of 30 s with Penalty-free RT range of 10 s. Minimum match factor applied was 60. The metabolites that were not identified in the Agilent Fiehn GC/MS Metabolomics RTL Library were searched in the National Institute of Standards and Technology library 11 (2014) using Unknowns-Agilent MassHunter Workstation Quantitative Analysis (version B.06.00).

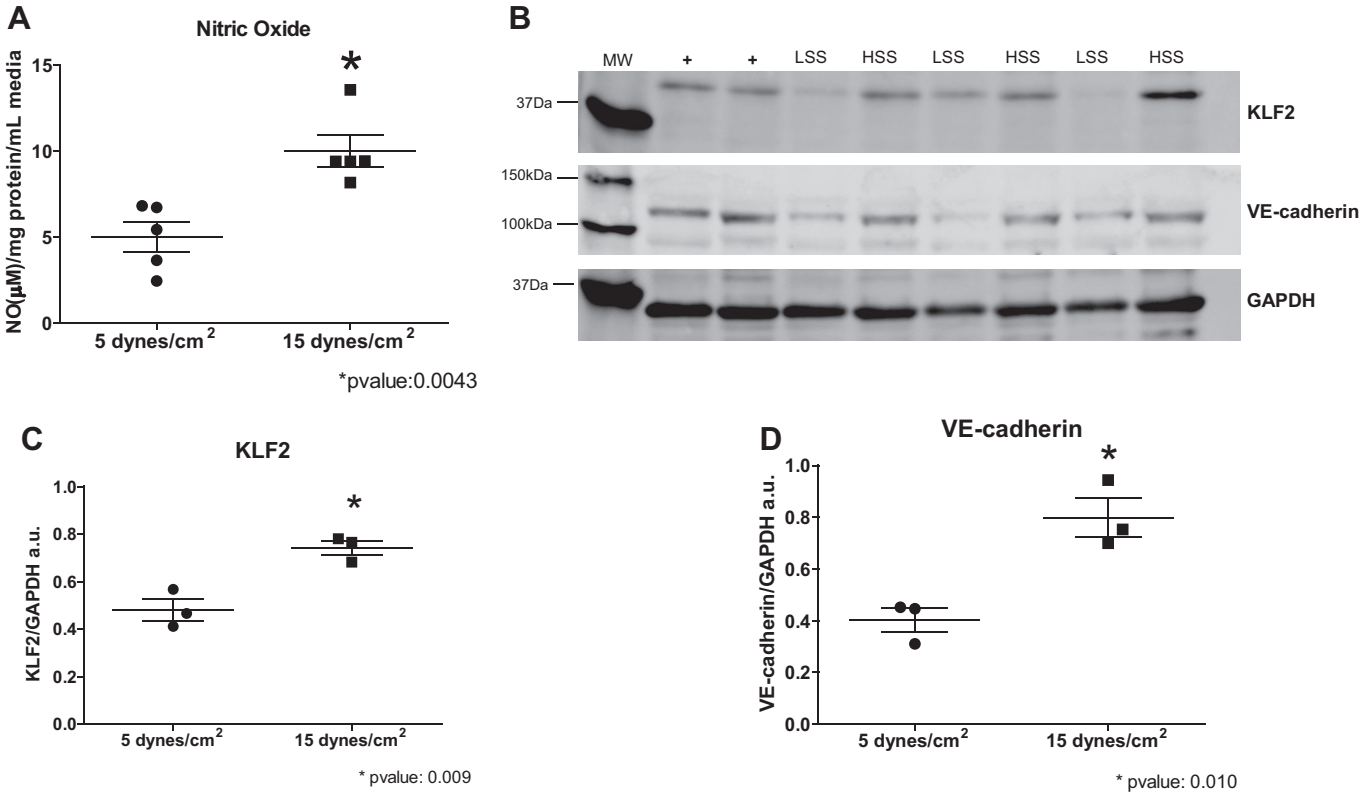

Fig. 1. Cells under high shear stress (HSS) flow (15 dyn/cm^2) released higher concentration of nitric oxide (NO) in medium (*A*) (measured through nitrate and nitrite intermediates, $n = 5$) and showed higher expression of KLF2 (*B* and *C*) and VE-cadherin (*B* and *D*) when compared with cells under low shear stress (LSS; 5 dyn/cm^2). Each dot represents a sample, lines represent means ± SE, and *P* values resulted from *t*-test. (+) Cells without starving as positive control. a.u., arbitrary units; KLF2, Krüppel-like factor 2.

Data consistency was checked based on the identification of Internal Standard (myristic acid d27) among samples, identification of each metabolite in at least two of three technical replicates and a coefficient variation of metabolites intensity <30% among the three technical replicates. Only metabolites that were present in at least ≤50% of samples from one group (LSS, HSS, or LSS with statin) were submitted to statistical analysis. Metabolites were analyzed using the MetaboAnalyst online platform (76). Missing values were substituted by the half of lower value in the table, and data were normalized using autoscaling method. Metabolite intensities were log2 transformed, and an ANOVA test was performed with Fisher's least significant difference as post hoc test. The metabolites that were different between groups were analyzed by principal component analysis. The mass spectrometry metabolomics data have been deposited to the Metabolights (28) repository with the data set identifier MTBLS739.

Subcellular fractioning. For enrichment of membrane and nucleus proteins, we used Subcellular Protein Fractionation Kit for Cultured Cells (no. 78840; Thermo Scientific) following the manufacturer's recommendation. Cells were submitted to HSS and LSS according to previous description and four samples ($n = 4$) were analyzed.

Western blotting. Proteins were extracted and quantified as described above (see *Protein extraction*). Ten micrograms of total protein were loaded in SDS-PAGE electrophoresis and transferred to PVDF membrane (no. 25006567; GE HybondP) in a semidry system. Membranes were blocked with 5% BSA in PBST solution and incubated overnight against the target antibodies glycosylated and nonglycosylated LDLR (no. LS-B10039; LSBio), KLF2 (no. LS-B4570; LSBio), and VE-cadherin (no. 2500; Cell Signaling). GAPDH (no. ab22555; Abcam) was used as loading control. After primary antibody incubation, membranes were incubated for 1 h with goat anti-rabbit IgG (H^+L) secondary antibody and horseradish peroxidase conjugated (no. 31460; Thermo Scientific). After the secondary antibody incubation, membranes were washed and stained with ECL solution. Membranes were then digitized on an ImageScanner LAS 4000 mini (GE HealthCare, Little Chalfont, UK) and quantified using ImageJ software (National Institutes of Health, Bethesda, MD).

Nitric oxide detection assay. The release of nitric oxide (NO) from HUVECs under SS for 24 h was measured as nitrite (NO_2^-) and nitrate (NO_3^-) accumulation in the culture media as previously described (6). We analyzed the chemiluminescence reaction between ozone and the NO generated by reduction of the sample with vanadium chloride in acid at 95°C using NO analyzer (model 208A; Sievers Instruments, Boulder, CO) according to the manufacturer's protocols. NO_2^- and NO_3^- levels were corrected for total protein content of HUVECs extracts and media volume. The rates of NO_2^- and NO_3^- accumulation are expressed as micromoles per grams of protein per milliliters of medium. Five samples were analyzed.

Immunofluorescence. After high and lose SS, cells were fixed with paraformaldehyde (no. 158127; Sigma-Aldrich) 4% diluted in PBS for 30 min. After washes, cells were blocked with 2% casein in PBS solution for 1 h at room temperature followed by incubation with primary LDLR antibody overnight at 4°C. After primary antibodies, cells were incubated with a secondary Alexa 555 antibody (no. A27039; Thermo Scientific) and DAPI (no. D9542; Sigma-Aldrich) for 90 min. Immunohistochemistry was analyzed on a Laser Scanning Microscope 510 (Carl Zeiss). Three samples were analyzed

Enrichment analysis. Proteins upregulated in each group were associated with canonical pathways using the statistical overrepresentation test from Panther (version 05/12/2017) (41, 42). Upregulated proteins from LSS or HSS were uploaded separately and associated with canonical pathways using *Homo sapiens* Reactome database as background (version 58 published in 12/07/2016). The association was performed using Fisher's exact test with correction for multiple testing (Benjamini and Hochberg false discovery rate) and $P < 0.05$. Network analysis between proteins was performed in NetworkAnalyst (75) using IMEX (8) protein-protein interaction database, and network analysis between metabolites-proteins was performed using the Network Explorer plugin in MetaboAnalyst platform. KEGG *Homo sapiens* database was used as background. Both networks were constructed with zero-order interaction using only statically significant metabolites/proteins.

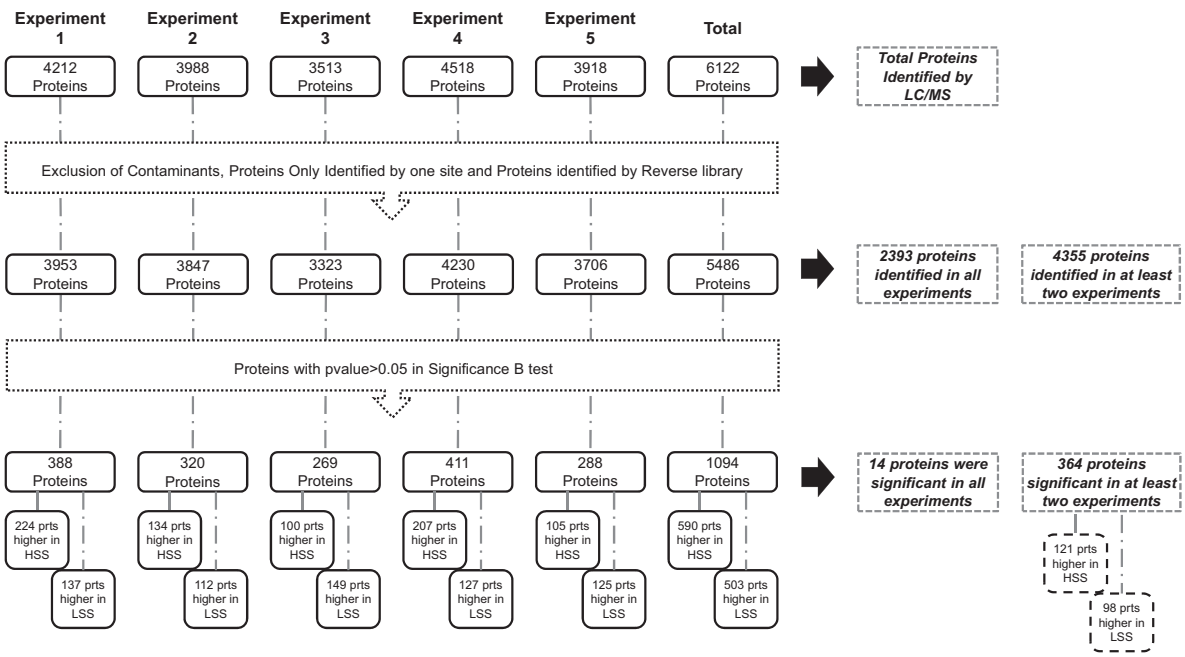

Fig. 2. Proteomic results overview. A total of 6,122 proteins were identified by mass spectrometry in all experiments. After contaminants and misidentification were filtered out, 5,486 proteins were used in statistical analysis. Of those, 1,094 proteins showed $P < 0.05$, and 364 were identified as significative in at least 2 biological replicates. A total of 121 proteins were upregulated in high shear stress (HSS) and 98 were upregulated in low shear stress (LSS). The upregulated proteins in each group were used in follow-up analysis. $n = 5$ Samples.

RESULTS

We performed HSS and LSS in five biological replicates in HUVECs between passage 8 and 10. As expected and well reported in the literature, we observed a significant increase in NO release in cells under HSS compared with LSS. In addition, we also observed upregulation of KLF2 and VE-cadherin in this same group (Fig. 1).

Lipid metabolism is downregulated in HUVECs under LSS. After mass spectrometry analysis and filters, we identified 5,486 proteins. From them, 1,094 showed a $P < 0.05$ in the significance B test. We considered for follow-up analysis proteins with $P < 0.05$ in the same direction and in at least 2 samples, resulting in 364 proteins. From these 364 proteins, 121 were higher in HSS (HSS/LSS ratio equal or higher than 1.25) and 98 were higher in LSS (LSS/HSS ratio equal or higher than 1.25). The total number and the number of significant proteins are summarized in Fig. 2. A heatmap of the 364 significant proteins was plotted in Fig. 3*A*. Despite the fact that we were working with HUVECs, we were able to identify several proteins known as markers of native endothelial cells such as ADGRL4, EMCN, ENG, PECAM1, TEK, TSPAN8, VGFR2, CD34, and VWF. The proteins identified in this study are listed in Supplemental Table S1 (see Supplemental Material: https://doi.org/10.6084/m9.figshare.7961018).

We performed enrichment analysis with the upregulated proteins in LSS and HSS. Two main pathways were upregulated in HSS: metabolism (parental pathway), specifically lipid and lipoprotein metabolism and metabolism of proteins (parental pathway), specifically *N*-glycosylation posttranslational modification (Fig. 3*B*, orange). In cells under LSS the upregulated proteins were related to adhesion molecules, extracellular matrix components, stress fibers, and platelet activation (Fig. 3*B*, blue).

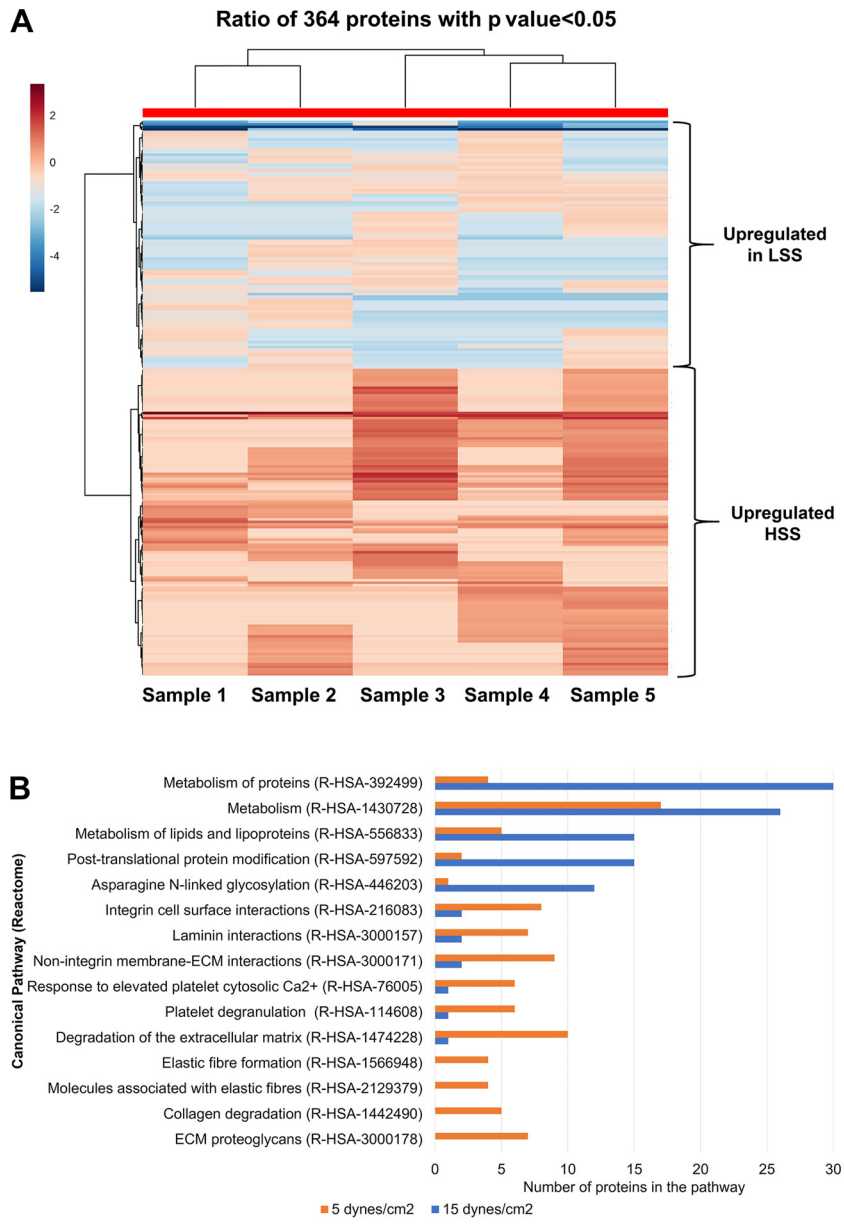

Fig. 3. *A*: heatmap of 364 proteins with $P < 0.05$ in significance B test in at least 2 replicates. Proteins were clustered into two main groups: upregulated in high shear stress (HSS; *bottom*, red) and upregulated in low shear stress (LSS; *top*, blue). In the heatmap it was plotted log2 of HSS/LSS ratio intensity. *B*: canonical pathways enriched by differential proteins of human umbilical vein endothelial cells (HUVECs) under LSS and HSS according to Panther Enrichment Analysis. Pathways such as lipid metabolism and protein metabolism were enriched in cells under HSS whereas pathways related to platelet activation, integrin signaling, extracellular matrix, and adhesion molecules were enriched in cells under LSS. Blue bars show the number of proteins enriched in HSS (15 dyn/cm^2), and orange bars show the number of proteins enriched in LSS (5 dyn/cm^2) in each pathway; $n = 5$ samples.

Table 1. *Proteins are part of upregulated canonical pathways in cells under HSS and LSS*

Reactome Pathway	No. of Proteins in Reference	Proteins Uploaded in Panther Enrichment Analysis	Expected	Fold Enrichment	Raw *P* Value	FDR *P* Value
1-Metabolism (R-HSA-1430728)	1,968	LDLR, HYAL2, MBOAT7, NCEH1, ELOVL1, SLC25A6, CAV1, CYB5R3, ATP5F1, AKR1C3, ACAT1, HMOX1, LPCAT2, SLC25A4, NQO1, CAT, ESYT1, MED4, AKR1C4, HSD17B12, VAPA, SULT1A3, AKR1C2, DHCR7, CD44, GLUD1	11.6	2.24	8.18×10^{-5}	1.25×10^{-2}
1.1-Metabolism of lipids and lipoproteins (R-HSA-556833)	712	ABCD3, ACAT1, AK1C2, AK1C3, AK1C4, CAV1, DHB12, DHCR7, ELOV1, ESYT1, LDLR, MBOA7, MED4, NCEH1, PCAT2, VAPA	4.2	3.58	2.35×10^{-5}	5.18×10^{-3}
2-Metabolism of proteins (R-HSA-392499)	1,325	GSN, SRPRA, SLC25A6, TMED9, ADAMTSL1, CD59, LMAN2, SLC25A4, TMED10, LMAN1, CKAP4, SEC61B, DNAJC3, SRPRB, RAB1A, MPDU1, SSR1, SPCS1, SULT1A3, VDAC1, SSR4, PIGS, SPCS2, SPCS3, MOGS	6.23	4.01	2.01×10^{-9}	4×10^{-6}
2.1-Posttranslational protein modification (R-HSA-597592)	819	RPN2, TMED9, CANX, ADAMTSL1, CD59, LMAN2, TMED10, LMAN1, RAB1A, MPDU1, RPN1, DDOST, VDAC1, PIGS, MOGS	4.83	3.11	1.11×10^{-4}	1.43×10^{-2}
2.2-Asparagine N-linked glycosylation (R-HSA-446203)	296	RPN2, TMED9, CANX, CD59, LMAN2, TMED10, LMAN1, RAB1A, MPDU1, RPN1, DDOST, MOGS	1.74	6.88	2.71×10^{-7}	8.99×10^{-5}
3-SRP-dependent cotranslational protein targeting to membrane (R-HSA-1799339)	112	RPN2, SRPRA, SEC61B, SRPRB, SSR1, RPN1, DDOST, SPCS1, SSR4, SPCS2, SPCS3	0.66	16.67	1.58×10^{-10}	3.14×10^{-7}
4-Laminin interactions (R-HSA-3000157)	30	LAMA4, NID1, HSPG2, COL18A1, LAMB1, LAMC1, COL4A2	0.14	50.1	3.40×10^{-10}	2.26×10^{-7}
5-Integrin cell surface interactions (R-HSA-216083)	85	COL5A1, HSPG2, FN1, COL8A1, COL18A1, THBS1, ICAM1, COL4A2	0.4	20.21	1.18×10^{-8}	4.68×10^{-6}
6-Nonintegrin membrane-ECM interactions (R-HSA-3000171)	59	LAMA4, COL5A1, HSPG2, FN1, THBS1, NTN4, LAMB1, LAMC1, COL4A2	0.27	32.75	2.67×10^{-11}	2.66×10^{-8}
7-Response to elevated platelet cytosolic Ca^{2+} (R-HSA-76005)	130	FN1, MMRN1, SERPINE1, THBS1, MAGED2, CLU	0.61	9.91	4.11×10^{-5}	8.18×10^{-3}
7.1-Platelet degranulation (R-HSA-114608)	125	FN1, MMRN1, SERPINE1, THBS1, MAGED2, CLU	0.58	10.31	3.33×10^{-5}	7.37×10^{-3}
8-Collagen biosynthesis and modifying enzymes (R-HSA-1650814)	67	COL5A1, COL12A1, COL8A1, COL18A1, COL4A2	0.31	16.02	2.11×10^{-5}	5.26×10^{-3}
9-Degradation of the extracellular matrix (R-HSA-1474228)	137	COL5A1, NID1, HSPG2, FN1, COL12A1, COL8A1, COL18A1, LAMB1, LAMC1, COL4A2	0.64	15.67	1.61×10^{-9}	8.02×10^{-7}
9.1-Collagen degradation (R-HSA-1442490)	64	COL5A1, COL12A1, COL8A1, COL18A1, COL4A2	0.3	16.77	1.72×10^{-5}	4.88×10^{-3}
10-Elastic fiber formation (R-HSA-1566948)	45	FN1, EFEMP1, EMILIN1, LTBP2	0.21	19.09	7.84×10^{-5}	1.20×10^{-2}
10.1-Molecules associated with elastic fibers (R-HSA-2129379)	38	FN1, EFEMP1, EMILIN1, LTBP2	0.18	22.6	4.25×10^{-5}	7.68×10^{-3}
11-ECM proteoglycans (R-HSA-3000178)	75	LAMA4, COL5A1, FN1, SERPINE1, LAMB1, LAMC1, COL4A2	0.35	20.04	1.06×10^{-6}	3.51×10^{-5}

FDR, false discovery rate; HSS, high shear stress; LSS, low shear stress.

Sixteen proteins participating in lipid transport, lipid biosynthesis, lipid oxidation, and lipid catabolism were upregulated in HSS and are listed in Table 1.

Supporting proteomic findings, metabolomic data also showed downregulation of lipids and lipid metabolites in LSS. Nine lipids were in lower concentration in LSS compared with HSS including cholesterol, palmitic acid, 13-docosenoic acid, octanoic acid, 2-methyl-pentenedioic acid, heptadecanoic acid, 1-heptanol, myo-inositol, and myo-inositol-1,2,4,5,6P (Fig. 4*A*).

In addition to lipids, metabolomic data also showed downregulation of 14 amino acids in LSS, including L-alanine, L-proline, L-serine, aspartic acid, aparagine, L-valine, glutamic acid, L-glutamine, L-methionine, L-lysine, L-glycine, L-threonine, L-Isoleucine, and tyrosine (Fig. 4*B*). We observed three proteins related to glutamate metabolism upregulated in HSS (PRFA3, DHE3, and NQO1) and two proteins upregulated in LSS, one part of serine synthesis pathway (SERC) and other from the arginine, proline and ornithine synthesis pathway (P5CS).

Three metabolites from the citric acid cycle were also modulated in SS, with succinic acid, malic acid, and fumaric acid upregulated in HSS (Fig. 4*B*).

LDLR showed different behaviors in HUVECs under LSS and HSS. Analyzing together the proteins and metabolites from lipid metabolism in a network, LDLR was the protein with the highest number of direct connections, connecting to CAV1, PDIA4, CANX, and Rab1A, also connected to cholesterol. In addition, cholesterol was the metabolite with the highest number of connections with proteins, connecting to Rab1A, NCEH1, ABCD3, DHCR7, and ACAT1.

Expectedly, based on our omics data, LDLR was downregulated in the membrane fraction of cells under LSS (Fig. 5*B*).

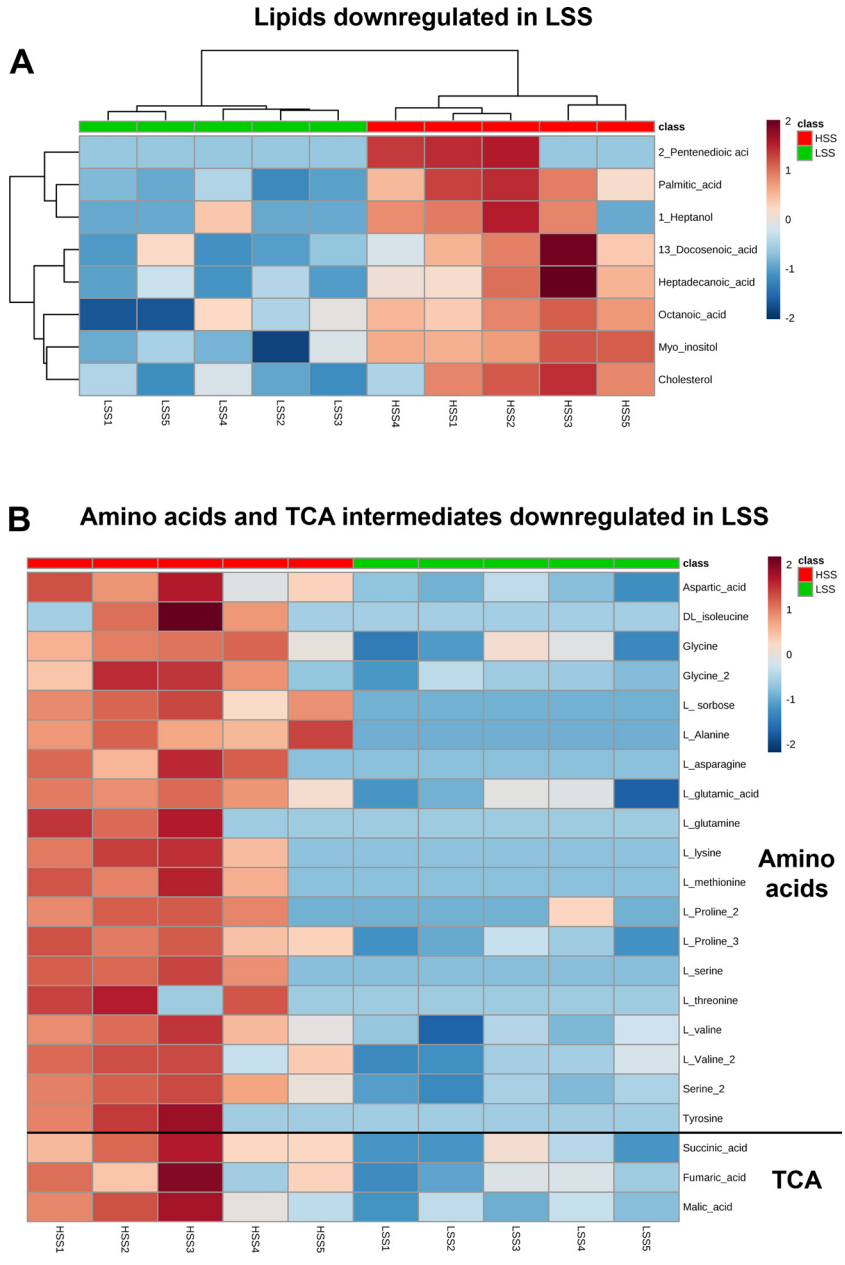

Fig. 4. Heatmap of metabolites different in human umbilical vein endothelial cells (HUVECs) under low shear stress (LSS) and high shear stress (HSS). *A*: lipid metabolism is downregulated in HUVECs under LSS. Cholesterol, palmitic acid, 13-docosenoic acid, octanoic acid, 2-methyl-pentenedioic acid, heptadecanoic acid, 1-heptanol, myo-inositol, and myo-inositol-1,2,4,5,6P showed significantly lower concentration in cells under LSS compared with HSS. *B*: amino acids and tricarboxylic acid (TCA) intermediates were also upregulated in HSS. All of these metabolites showed *t*-test $P < 0.05$. Heatmap colors represent a z-score (-2 to 2) log2 normalized of metabolite intensity.

Unexpectedly, LDLR showed in a nonglycosylated form (precursor form with lower molecular weight) in cells under LSS, whereas in HSS we only identified receptors in the glycosylated form (mature form) (Fig. 5*A*). In addition, according to immunofluorescence analysis, LDLR was located around the nuclei in cells under LSS while in HSS the receptor was widely distributed throughout the membrane (Fig. 5*C*).

In addition to the presence of nonglycosylated LDLR in cells under LSS, we also identified decreased expression of proteins essential to the glycosylation process. RPN1, RPN2, and DDOST are all subunits of the catalytic core of *N*-oligosaccharyl transferase (OST), and they are upregulated in cells under HSS, suggesting that the glycosylation process could be impaired in HUVECs under atheroprone flow.

Statin treatment in LSS cells is able to partly recover the protective phenotype seen in HSS. Based on the observed modulation of LDLR in different SS intensities, we decided to modulate this protein using a pharmacological and translational approach. HUVECs were treated with atorvastatin over 72 h to increase LDLR expression and then submitted to LSS. However, the metabolite profile of HUVECs under LSS and HSS was different after atorvastatin treatment: the metabolite profile of treated LSS cells was closer to the one of untreated cells under HSS (Fig. 6). Upregulation of LDLR in LSS resulted in an increase in lipid metabolite levels such as palmitic acid, octanoic acid, and 2-methyl-pentenedioic acid; amino acids such as L-asparagine and L-serine; carboxylic acids such as succinic acid and oxalic acid; the sugars altrose, allose, sorbose, and α-mannobiose; and others such as xanthotoxin and 4-bromo-1-butanol (Fig. 7,). These metabolites were statistically different between cells under HSS and LSS ($P < 0.05$), but no difference was observed after atorvastatin treatment. We did not observe any difference in these results when cells where treated with both atorvastatin and nitro-L-arginine methyl ester (since atorvastatin treatment results in the increase of NO release as well as LDLR upregulation (3, 21, 38, 39).

We also observed the same behavior in myo-inositol, 2,5-furandicarboxylic acid, glycine, and glutamic acid . However,

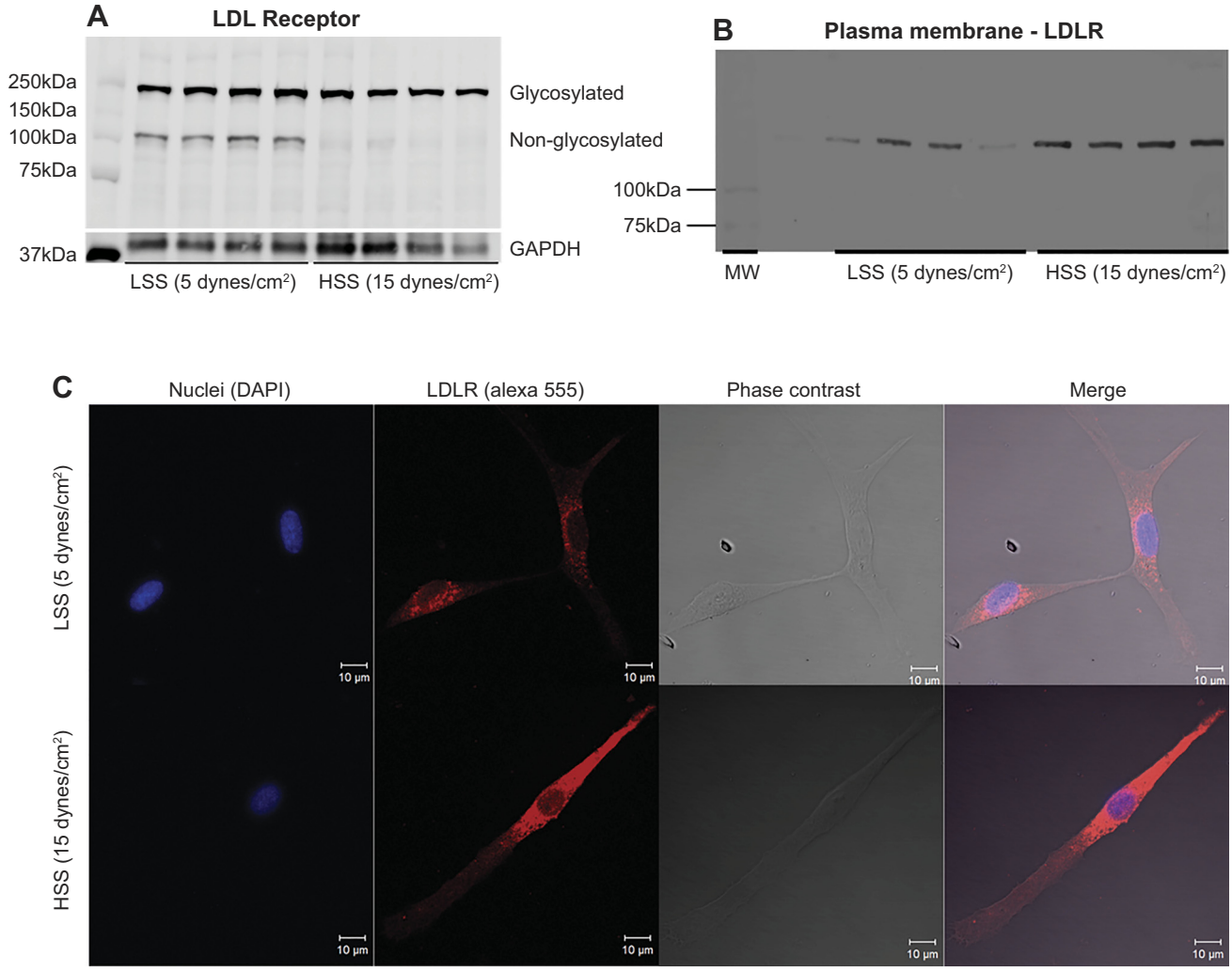

Fig. 5. Low-density lipoprotein receptor (LDLR) is modulated in endothelial cells under low shear stress (LSS) and high shear stress (HSS). *A*: human umbilical vein endothelial cells (HUVECs) under LSS showed part of the receptors in nonglycosylated form, whereas cells under HSS showed the LDLR only in glycosylated form; $n = 4$ samples. *B*: LDLR is downregulated in membrane fraction of cells under LSS compared with HSS; $n = 4$ samples. *C*: immunofluorescence showing that, in cells under LSS, the LDLR is located around nuclei and in HSS, it is distributed in cell membrane. Blue: nuclei; red: LDLR; green: autofluorescence of elastic lamina. Scale bar = 10 μm; representative images of $n = 3$ samples.

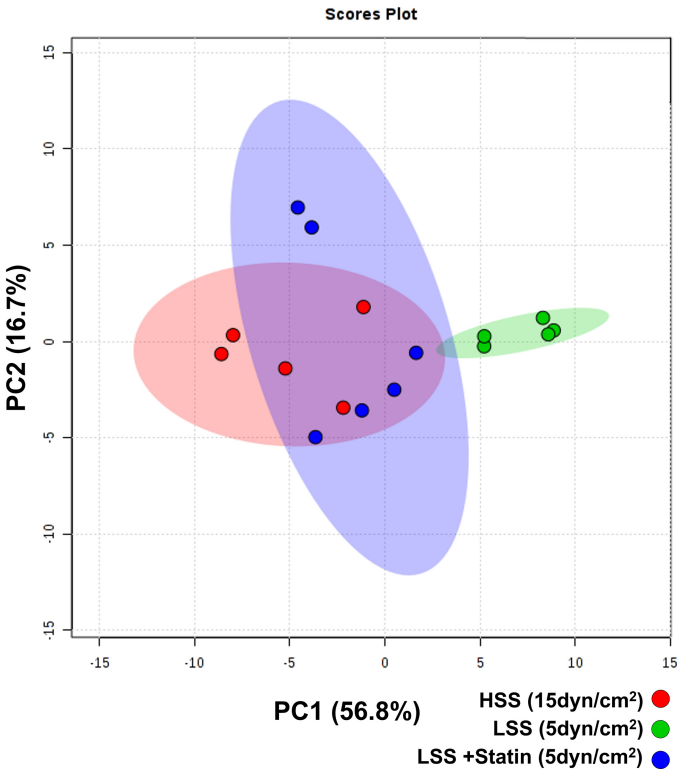

Fig. 6. Scores plot of principal component analysis of cells under high shear stress (HSS; red), cells under low shear stress (LSS; green), and cells under LSS plus atorvastatin treatment (blue). PC1 and PC2: principal component 1 and principal component 2. Each point represents a metabolite profile of a biological replicate.

the values decreased when we treated cells with atorvastatin plus nitro-L-arginine methyl ester suggesting that these metabolite responses to atorvastatin were modulated by NO levels and not by LDLR upregulation (Fig. 7).

DISCUSSION

The present work used the integration of proteomics and metabolomics data from HUVECs under LSS and HSS to identify the pathways and mechanisms behind the atheroprone and atheroprotector phenotype adopted by ECs under different flow conditions.

Overall lipid metabolism is deficient in our model. We show lipid biosynthesis to be compromised in HUVECs under atheroprone flow and associated with decreased expression of several key enzymes from the pathway. Associated with this, we show a lower level of mature LDLR in the cellular membrane. Finally, the increase in membrane LDLR with statin was able to partially recover the atheroprotector phenotype in cells under LSS suggesting a mechanism for the well-known statin effect regardless of total circulating cholesterol reductions.

Despite the limitation of using HUVECs as a model, we believe HUVECs are representatives of native endothelial cells at the proteomics level since we were able to identify by mass spectrometry several proteins that are known as endothelial cell markers such as ADGRL4, EMCN, ENG, PECAM1, TEK, TSPAN8, VGFR2, CD34, and VWF. Also, using our in vitro model we identified the same previously described upregulation of adhesion molecules, inflammatory pathway proteins and procoagulation factors in cells under LSS (1, 13, 14, 49, 64).

In addition, we found three proteins from the Hippo-YAP-Taz pathway upregulated after 24 h of LSS: CTGF, CYR61, and WWTR1. Our data corroborate with the literature (51, 75, 81) showing downregulation of YAP pathway proteins in long-term HSS and activation when cells are under LSS. It is important to highlight previous work showing activation of YAP signaling in endothelial cells under laminar SS in the first minutes of stimuli (after 10 min). The same authors also showed a decrease in YAP signaling in long-term SS (below static condition after 6 and 24 h), with YAP exclusion from nuclei after 6 h or 24 h of the laminar SS, followed by a decreasing in the expression of CTGF and CYR61. The authors suggest the mechanosensory role of these molecules in atheroprone phenotype of endothelial cells, acting as triggers of the inflammatory phenotype in the beginning of atherosclerosis developent. The literature also suggested transient role of YAP-Taz signaling in other phenotypes modulated by flow such as cell migration (40), cell cycle (41), and vessel maintenance (51) with upregulation of the signaling in the begging of SS stimuli and downregulation in long term. Our data suggest the YAP signaling is related not only with SS stimuli but also with flow intensity.

The upregulated pathways of LSS found in our work corroborate mechanisms previously described. Unexpectedly, however, the most enriched pathway in HSS in our system was none of these. Rather, we identify lipid metabolism as the top modulated pathway.

Lipid metabolism was downregulated in LSS in comparison to cells under HSS. Among the proteins downregulated in LSS, those that participate in cholesterol metabolism, both synthesis and degradation, were affected by SS intensity. This result was found not only through protein analysis but also in metabolomic analysis showing the downregulation of cholesterol, palmitic acid, palmitoleic acid and myristic acid after 24 h of LSS. Modulation of lipid metabolism with statin treatment partially recovered the atheroprotector phenotype in cells under LSS.

Our data suggest that LDLR may have an important role in this process. We show that LDLR is partially nonglycosylated

Fig. 7. Metabolites were downregulated in cells under low shear stress (LSS; 5 dyn/cm^2) compared with high shear stress (HSS; 15 dyn/cm^2) and recovered their value after low-density lipoprotein receptor (LDLR) modulation (5 dyn/cm^2 plus statin). *A–D*: lipids palmitic acid, octanoic acid, and 2-methyl-pentenedioic acid (*A*); amino acids L-asparagine, and L-serine (*B*); carboxylic acid succinic acid and oxalic acid (*C*); and sugars altrose, allose, sorbose, and α-mannobiose and others such as xanthotoxin and 4-bromo-1-butanol (*D*) were statistically downregulated in cells under LSS compared with HSS and were upregulated after atorvastatin treatment. *E*: myo-inositol, glycine, glutamic acid, and 2,5-furandicarboxylic acid showed the same behavior; however, values decreased when cells were treated with atorvastatin plus nitro-L-arginine methyl ester, suggesting that these metabolite responses to atorvastatin were modulated by nitric oxide (NO) levels. Metabolite intensity is plotted on the *y*-axis, and intensity was measured by height of chromatography peak and normalized by protein concentration. ANOVA with Bonferroni post hoc test was applied. Each dot represents a sample, and lines represent means ± SE; $n = 6$ samples.

Metabolites recovered HSS levels after statin treatment

A - Lipids

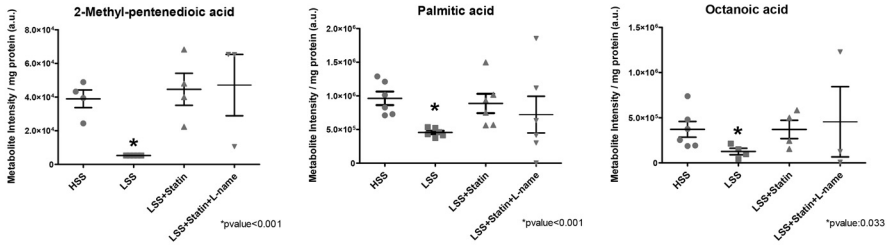

B - Amino acids

C - Carboxylic acids

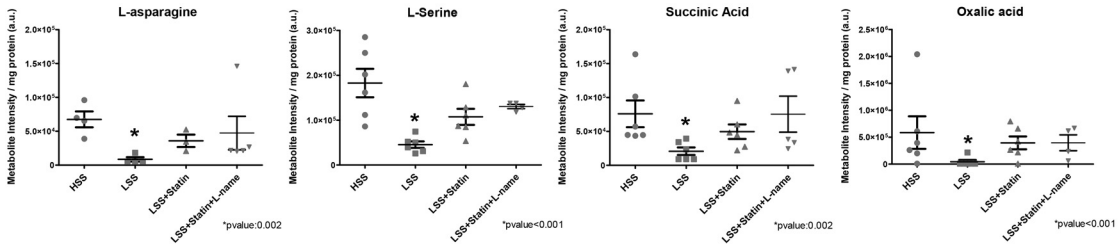

D- Sugars and other

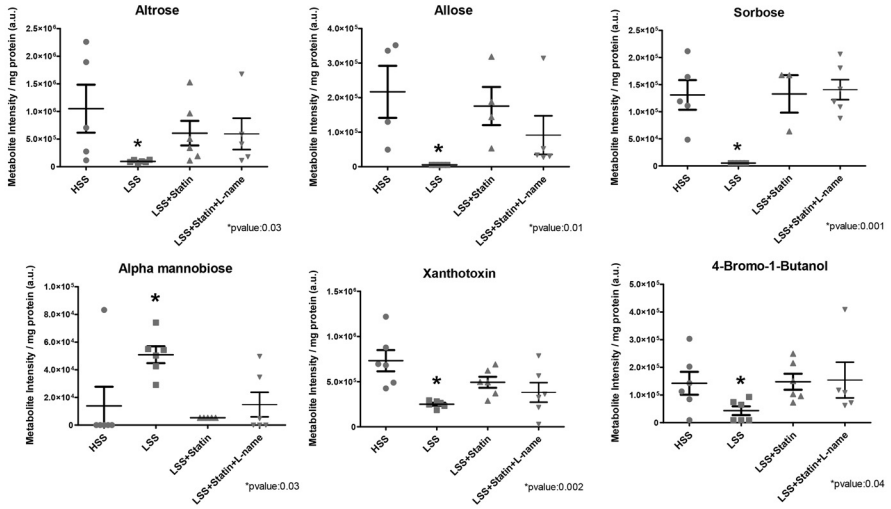

E- Statin effect NO dependent

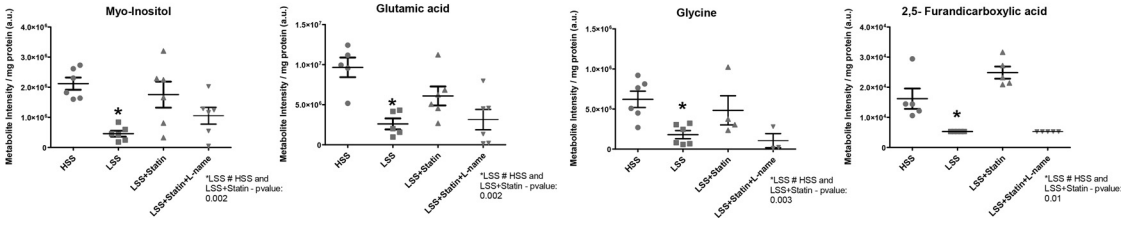

(precursor form) in cells under LSS, whereas in cells under HSS we only detect the glycosylated form of the protein (mature form) (Fig. 5). The receptor showed lower levels in the membrane of cells under LSS and distributed around the nuclei in atheroprone flow, whereas in HSS the receptor was increased in HUVECs and homogenously distributed throughout the membrane.

Goldstein and Brown described in 1983 (9) the LDLR to be downregulated in branch areas of the vasculature and hypothesized that this fact could have a role in atherosclerosis development. At the same time, Sprague and collaborators (65) showed that cells under HSS incorporated more LDL in comparison to cells under LSS. They also showed that cells under HSS had higher expression of LDLR and LDL incorporation suggesting the receptor could be modulated by flow (65). Nonetheless, few papers explored the association of LDLR and SS after the 1980s, and only in 2002, Liu and collaborators (40) showed SREBP1, a transcriptional factor associated with LDLR expression, to be higher in cells under HSS in comparison to a static condition.

The LDLR is a single-pass transmembrane receptor present in the cell surface, and it is the main receptor involved in LDL metabolism (25, 44, 46, 50). The receptor shows many post-translational modifications, including various sites of *N*- and *O*-glycosylation (18, 36, 57). LDLR is synthetized in a precursor form that becomes mature after the addition of carbohydrate chains, more precisely, 2 *N*-linked glycosylations and 18 *O*-linked glycosylations (16). Literature data show LDLR glycosylation to be essential for receptor cellular surface expression and stability (35, 36); cells with defects in LDLR glycosylation presented 5- to 10-fold faster degradation. It has also been suggested that glycans protect the receptor against degradation and could promote the binding of the receptor with other molecules such as those participating in LDLR transport (60, 78).

In our data, the differences between precursor and mature forms of the LDLR in cells under different SS conditions were concomitant with the downregulation of proteins involved in the glycosylation process. In fact, the four essential catalytic subunits of OST (RPN1, RPN2, and DDOST) were decreased in cells under LSS. Besides these three proteins, we identified other proteins from the endoplasmic reticulum to be decreased in cells under LSS. Recent findings show endoplasmic reticulum stress in atheroprone SS to be an initiator of the downstream regulation of the inflammatory process (2, 54). In this sense, abnormalities in LDLR glycosylation could be the result of endoplasmic reticulum stress since this is an important compartment of the glycosylation process.

Our data show a downregulation of cholesterol concomitant with the downregulation of LDLR. Changes in cholesterol membrane composition were already observed in cells under different intensities of SS (10, 77) and were associated with changes in membrane fluidity. However, cholesterol is also important in cellular signaling being part of the lipid rafts (62). Recent data showed SS-modulated molecules to be located in lipid rafts. In addition, changes in the membrane cholesterol level were shown to lead to impairment of membrane structure and activation of many signaling molecules (24, 27, 55, 72). Adhesion proteins such as VCAM-1 and ICAM-1 and inflammatory molecules such as caspase-1 and IL-1β are downstream molecules in pathways associated with SS, and they have been described as modulated by cholesterol content in lipid rafts (66).

Pharmacological modulation of LDLR levels with statin recapitulated the HSS metabolic phenotype of ECs under LSS. Statins are inhibitors of HMG-CoA reducing cholesterol biosynthesis and increasing LDLR expression . It is well known that statin treatment has benefits beyond the reduction of circulating cholesterol levels. Our data suggest that part of this benefit may derive locally, from changing the endothelial metabolic phenotype. Indeed, the local benefits of statin on endothelial cells are reported in the literature, such as affecting HUVECs growth and migration by mechanisms that are not directly associated with cholesterol. Despite local in nature, we were able to show that at least part of the statin reversion of the LSS phenotype can be associated with LDLR modulation and not with other effects of statins such as those associated with NO upregulation (3). Nonetheless, it is still possible that part of the described effects may be due to modulation of other unknown pathways also modulated by statin treatment.

In addition to lipids, we identified downregulation of amino acids and tricarboxylic acid (TCA) intermediates in LSS. All 14 amino acids that were identified in lower concentration could participate as carbon source in anaplerotic reactions, producing gluconeogenic or ketogenic precursors and keeping the synthesis of TCA intermediates at almost normal levels (52). New experiments using carbon flow analysis or enzyme activity could help to better understand the decrease in amino acids in LSS. Despite our identification of metabolites from different classes, one limitation of the metabolomics methods we applied is the lack of measurement of some signaling lipids such as phospholipids.

Overall, the SS and atherosclerosis relationship is well described. However, how to modulate the atheroprone SS phenotype to a protector one is still a challenge. Our experiments using new "omics" techniques have been able to aggregate information to former theories, bringing old and new molecules back to the scene, which were not possible to be detected in the past.

ACKNOWLEDGMENTS

We thank Ana L. Garippo, Laura Ventura, Jessica Salgueiro, and Vanderbilt Mass Spectrometry Research Center for technical support.

GRANTS

This work was supported in part by Fundação de Amparo à Pesquisa do Estado de São Paulo (FAPESP Grants 2013/13526-0, 2016/02406-2, and 2013/17368-0); Financiadora de Inovação e Pesquisa (FINEP); Conselho Nacional de Desenvolvimento Cientifico e Tecnológico (CNPq); and Fundação Zerbini.

DISCLOSURES

No conflicts of interest, financial or otherwise, are declared by the authors.

AUTHOR CONTRIBUTIONS

G.V. and A.C.P. conceived and designed research; G.V., P.A.M., K.P., L.Y.T., R.D., V.M.C., and K.H.M.C. performed experiments; G.V., P.A.M., K.P., V.M.C., and K.H.M.C. analyzed data; G.V., P.A.M., F.R.L., R.D., J.E.K., and A.C.P. interpreted results of experiments; G.V. prepared figures; G.V. and A.C.P. drafted manuscript; G.V., J.E.K., and A.C.P. edited and revised manuscript; F.R.L. and A.C.P. approved final version of manuscript.

REFERENCE

1. **Ajami NE, Gupta S, Maurya MR, Nguyen P, Li JY, Shyy JY, Chen Z, Chien S, Subramaniam S.** Systems biology analysis of longitudinal

functional response of endothelial cells to shear stress. *Proc Natl Acad Sci USA* 114: 10990–10995, 2017. doi:10.1073/pnas.1707517114.

2. **Bailey KA, Haj FG, Simon SI, Passerini AG.** Atherosusceptible shear stress activates endoplasmic reticulum stress to promote endothelial inflammation. *Sci Rep* 7: 8196, 2017. doi:10.1038/s41598-017-08417-9.
3. **Bao XC, Mao AR, Fang YQ, Fan YH, Wang FF, Ma J, You P.** Simvastatin decreases hyperbaric oxygen-induced acute lung injury by upregulating eNOS. *Am J Physiol Lung Cell Mol Physiol* 314: L287–L297, 2018. doi:10.1152/ajplung.00520.2016.
5. **Barauna VG, Magalhaes FC, Campos LC, Reis RI, Kunapuli SP, Costa-Neto CM, Miyakawa AA, Krieger JE.** Shear stress-induced Ang II AT1 receptor activation: G-protein dependent and independent mechanisms. *Biochem Biophys Res Commun* 434: 647–652, 2013. doi:10.1016/j.bbrc.2013.04.005.
6. **Bassaneze V, Barauna VG, Lavini-Ramos C, Kalil J, Schettert IT, Miyakawa AA, Krieger JE.** Shear stress induces nitric oxide-mediated vascular endothelial growth factor production in human adipose tissue mesenchymal stem cells. *Stem Cells Dev* 19: 371–378, 2010. doi:10.1089/scd.2009.0195.
7. **Bendall SC, Hughes C, Stewart MH, Doble B, Bhatia M, Lajoie GA.** Prevention of amino acid conversion in SILAC experiments with embryonic stem cells. *Mol Cell Proteomics* 7: 1587–1597, 2008. doi:10.1074/mcp.M800113-MCP200.
8. **Breuer K, Foroushani AK, Laird MR, Chen C, Sribnaia A, Lo R, Winsor GL, Hancock RE, Brinkman FSL, Lynn DJ.** InnateDB: systems biology of innate immunity and beyond–recent updates and continuing curation. *Nucleic Acids Res* 41: D1228–D1233, 2013. doi:10.1093/nar/gks1147.
9. **Brown MS, Goldstein JL.** Lipoprotein metabolism in the macrophage: implications for cholesterol deposition in atherosclerosis. *Annu Rev Biochem* 52: 223–261, 1983. doi:10.1146/annurev.bi.52.070183.001255.
10. **Butler PJ, Norwich G, Weinbaum S, Chien S.** Shear stress induces a time- and position-dependent increase in endothelial cell membrane fluidity. *Am J Physiol Cell Physiol* 280: C962–C969, 2001. doi:10.1152/ajpcell.2001.280.4.C962.
11. **Caro CG, Fitz-Gerald JM, Schroter RC.** Arterial wall shear and distribution of early atheroma in man. *Nature* 223: 1159–1161, 1969. doi:10.1038/2231159a0.
12. **Chien S.** Mechanotransduction and endothelial cell homeostasis: the wisdom of the cell. *Am J Physiol Heart Circ Physiol* 292: H1209–H1224, 2007. doi:10.1152/ajpheart.01047.2006.
13. **Chistiakov DA, Orekhov AN, Bobryshev YV.** Effects of shear stress on endothelial cells: go with the flow. *Acta Physiol (Oxf)* 219: 382–408, 2017. doi:10.1111/apha.12725.
14. **Chiu JJ, Chien S.** Effects of disturbed flow on vascular endothelium: pathophysiological basis and clinical perspectives. *Physiol Rev* 91: 327–387, 2011. doi:10.1152/physrev.00047.2009.
15. **Cox J, Matic I, Hilger M, Nagaraj N, Selbach M, Olsen JV, Mann M.** A practical guide to the MaxQuant computational platform for SILAC-based quantitative proteomics. *Nat Protoc* 4: 698–705, 2009. doi:10.1038/nprot.2009.36.
16. **Cummings RD, Kornfeld S, Schneider WJ, Hobgood KK, Tolleshaug H, Brown MS, Goldstein JL.** Biosynthesis of N- and O-linked oligosaccharides of the low density lipoprotein receptor. *J Biol Chem* 258: 15261–15273, 1983.
17. **Davies PF.** Flow-mediated endothelial mechanotransduction. *Physiol Rev* 75: 519–560, 1995. doi:10.1152/physrev.1995.75.3.519.
18. **Davis CG, Elhammer A, Russell DW, Schneider WJ, Kornfeld S, Brown MS, Goldstein JL.** Deletion of clustered O-linked carbohydrates does not impair function of low density lipoprotein receptor in transfected fibroblasts. *J Biol Chem* 261: 2828–2838, 1986.
19. **Dewey CF Jr, Bussolari SR, Gimbrone MA Jr, Davies PF.** The dynamic response of vascular endothelial cells to fluid shear stress. *J Biomech Eng* 103: 177–185, 1981. doi:10.1115/1.3138276.
20. **Dimmeler S, Hermann C, Galle J, Zeiher AM.** Upregulation of superoxide dismutase and nitric oxide synthase mediates the apoptosis-suppressive effects of shear stress on endothelial cells. *Arterioscler Thromb Vasc Biol* 19: 656–664, 1999. doi:10.1161/01.ATV.19.3.656.
21. **Endres M, Laufs U, Huang Z, Nakamura T, Huang P, Moskowitz MA, Liao JK.** Stroke protection by 3-hydroxy-3-methylglutaryl (HMG)-CoA reductase inhibitors mediated by endothelial nitric oxide synthase. *Proc Natl Acad Sci USA* 95: 8880–8885, 1998. doi:10.1073/pnas.95.15.8880.
22. **Fan Y, Lu H, Liang W, Hu W, Zhang J, Chen YE.** Krüppel-like factors and vascular wall homeostasis. *J Mol Cell Biol* 9: 352–363, 2017. doi:10.1093/jmcb/mjx037.
23. **Feng S, Bowden N, Fragiadaki M, Souilhol C, Hsiao S, Mahmoud M, Allen S, Pirri D, Ayllon BT, Akhtar S, Thompson AA, Jo H, Weber C, Ridger V, Schober A, Evans PC.** Mechanical activation of hypoxia-inducible factor 1α drives endothelial dysfunction at atheroprone sites. *Arterioscler Thromb Vasc Biol* 37: 2087–2101, 2017. doi:10.1161/ATVBAHA.117.309249.
24. **Ferraro JT, Daneshmand M, Bizios R, Rizzo V.** Depletion of plasma membrane cholesterol dampens hydrostatic pressure and shear stress-induced mechanotransduction pathways in osteoblast cultures. *Am J Physiol Cell Physiol* 286: C831–C839, 2004. doi:10.1152/ajpcell.00224.2003.
25. **Finkelshtein D, Werman A, Novick D, Barak S, Rubinstein M.** LDL receptor and its family members serve as the cellular receptors for vesicular stomatitis virus. *Proc Natl Acad Sci USA* 110: 7306–7311, 2013. doi:10.1073/pnas.1214441110.
26. **Frank PG, Woodman SE, Park DS, Lisanti MP.** Caveolin, caveolae, and endothelial cell function. *Arterioscler Thromb Vasc Biol* 23: 1161–1168, 2003. doi:10.1161/01.ATV.0000070546.16946.3A.
27. **Fu Y, Hou Y, Fu C, Gu M, Li C, Kong W, Wang X, Shyy JY, Zhu Y.** A novel mechanism of γ/δ T-lymphocyte and endothelial activation by shear stress: the role of ecto-ATP synthase β chain. *Circ Res* 108: 410–417, 2011. doi:10.1161/CIRCRESAHA.110.230151.
28. **Haug K, Salek RM, Conesa P, Hastings J, de Matos P, Rijnbeek M, Mahendraker T, Williams M, Neumann S, Rocca-Serra P, Maguire E, González-Beltrán A, Sansone SA, Griffin JL, Steinbeck C.** MetaboLights–an open-access general-purpose repository for metabolomics studies and associated meta-data. *Nucleic Acids Res* 41, *D1*: D781–D786, 2013. doi:10.1093/nar/gks1004.
29. **Helmke BP, Goldman RD, Davies PF.** Rapid displacement of vimentin intermediate filaments in living endothelial cells exposed to flow. *Circ Res* 86: 745–752, 2000. doi:10.1161/01.RES.86.7.745.
30. **Himburg HA, Grzybowski DM, Hazel AL, LaMack JA, Li XM, Friedman MH.** Spatial comparison between wall shear stress measures and porcine arterial endothelial permeability. *Am J Physiol Heart Circ Physiol* 286: H1916–H1922, 2004. doi:10.1152/ajpheart.00897.2003.
31. **Hsieh HJ, Liu CA, Huang B, Tseng AH, Wang DL.** Shear-induced endothelial mechanotransduction: the interplay between reactive oxygen species (ROS) and nitric oxide (NO) and the pathophysiological implications. *J Biomed Sci* 21: 3, 2014. doi:10.1186/1423-0127-21-3.
32. **Jia X, Yang J, Song W, Li P, Wang X, Guan C, Yang L, Huang Y, Gong X, Liu M, Zheng L, Fan Y.** Involvement of large conductance Ca(2+)-activated K (+) channel in laminar shear stress-induced inhibition of vascular smooth muscle cell proliferation. *Pflugers Arch* 465: 221–232, 2013. doi:10.1007/s00424-012-1182-z.
33. **Jiu Y, Lehtimäki J, Tojkander S, Cheng F, Jäälinoja H, Liu X, Varjosalo M, Eriksson JE, Lappalainen P.** Bidirectional Interplay between Vimentin Intermediate Filaments and Contractile Actin Stress Fibers. *Cell Rep* 11: 1511–1518, 2015. doi:10.1016/j.celrep.2015.05.008.
34. **De Keulenaer GW, Chappell DC, Ishizaka N, Nerem RM, Alexander RW, Griendling KK.** Oscillatory and steady laminar shear stress differentially affect human endothelial redox state: role of a superoxide-producing NADH oxidase. *Circ Res* 82: 1094–1101, 1998. doi:10.1161/01.RES.82.10.1094.
35. **Kingsley DM, Kozarsky KF, Hobbie L, Krieger M.** Reversible defects in O-linked glycosylation and LDL receptor expression in a UDP-Gal/UDP-GalNAc 4-epimerase deficient mutant. *Cell* 44: 749–759, 1986. doi:10.1016/0092-8674(86)90841-X.
36. **Kozarsky K, Kingsley D, Krieger M.** Use of a mutant cell line to study the kinetics and function of O-linked glycosylation of low density lipoprotein receptors. *Proc Natl Acad Sci USA* 85: 4335–4339, 1988. doi:10.1073/pnas.85.12.4335.
37. **Lanucara F, Eyers CE.** Mass spectrometric-based quantitative proteomics using SILAC. *Methods Enzymol* 500: 133–150, 2011. doi:10.1016/B978-0-12-385118-5.00008-6.
38. **Laufs U, La Fata V, Plutzky J, Liao JK.** Upregulation of endothelial nitric oxide synthase by HMG CoA reductase inhibitors. *Circulation* 97: 1129–1135, 1998. doi:10.1161/01.CIR.97.12.1129.
39. **Laufs U, Liao JK.** Post-transcriptional regulation of endothelial nitric oxide synthase mRNA stability by Rho GTPase. *J Biol Chem* 273: 24266–24271, 1998. doi:10.1074/jbc.273.37.24266.

40. **Liu Y, Chen BP, Lu M, Zhu Y, Stemerman MB, Chien S, Shyy JY.** Shear stress activation of SREBP1 in endothelial cells is mediated by integrins. *Arterioscler Thromb Vasc Biol* 22: 76–81, 2002. doi:10.1161/hq0102.101822.
41. **Mi H, Muruganujan A, Casagrande JT, Thomas PD.** Large-scale gene function analysis with the PANTHER classification system. *Nat Protoc* 8: 1551–1566, 2013. doi:10.1038/nprot.2013.092.
42. **Mi H, Poudel S, Muruganujan A, Casagrande JT, Thomas PD.** PANTHER version 10: expanded protein families and functions, and analysis tools. *Nucleic Acids Res* 44, *D1*: D336–D342, 2016. doi:10.1093/nar/gkv1194.
43. **Mohan S, Mohan N, Sprague EA.** Differential activation of NF-κB in human aortic endothelial cells conditioned to specific flow environments. *Am J Physiol Cell Physiol* 273: C572–C578, 1997. doi:10.1152/ajpcell.1997.273.2.C572.
44. **Molina S, Castet V, Fournier-Wirth C, Pichard-Garcia L, Avner R, Harats D, Roitelman J, Barbaras R, Graber P, Ghersa P, Smolarsky M, Funaro A, Malavasi F, Larrey D, Coste J, Fabre JM, Sa-Cunha A, Maurel P.** The low-density lipoprotein receptor plays a role in the infection of primary human hepatocytes by hepatitis C virus. *J Hepatol* 46: 411–419, 2007. doi:10.1016/j.jhep.2006.09.024.
45. **Mun GI, Boo YC.** A regulatory role of Kruppel-like factor 4 in endothelial argininosuccinate synthetase 1 expression in response to laminar shear stress. *Biochem Biophys Res Commun* 420: 450–455, 2012. doi:10.1016/j.bbrc.2012.03.016.
46. **Nagajyothi F, Weiss LM, Silver DL, Desruisseaux MS, Scherer PE, Herz J, Tanowitz HB.** Trypanosoma cruzi utilizes the host low density lipoprotein receptor in invasion. *PLoS Negl Trop Dis* 5: e953, 2011. doi:10.1371/journal.pntd.0000953.
47. **Nakajima H, Mochizuki N.** Flow pattern-dependent endothelial cell responses through transcriptional regulation. *Cell Cycle* 16: 1893–1901, 2017. doi:10.1080/15384101.2017.1364324.
49. **Novodvorsky P, Chico TJ.** The role of the transcription factor KLF2 in vascular development and disease. *Prog Mol Biol Transl Sci* 124: 155–188, 2014. doi:10.1016/B978-0-12-386930-2.00007-0.
50. **Olofsson S, Bergström T.** Glycoconjugate glycans as viral receptors. *Ann Med* 37: 154–172, 2005. doi:10.1080/07853890510007340.
51. **Ong SE, Mann M.** A practical recipe for stable isotope labeling by amino acids in cell culture (SILAC). *Nat Protoc* 1: 2650–2660, 2006. doi:10.1038/nprot.2006.427.
52. **Owen OE, Kalhan SC, Hanson RW.** The key role of anaplerosis and cataplerosis for citric acid cycle function. *J Biol Chem* 277: 30409–30412, 2002. doi:10.1074/jbc.R200006200.
53. **Pahakis MY, Kosky JR, Dull RO, Tarbell JM.** The role of endothelial glycocalyx components in mechanotransduction of fluid shear stress. *Biochem Biophys Res Commun* 355: 228–233, 2007. doi:10.1016/j.bbrc.2007.01.137.
54. **Pan L, Hong Z, Yu L, Gao Y, Zhang R, Feng H, Su L, Wang G.** Shear stress induces human aortic endothelial cell apoptosis via interleukin-1 receptor-associated kinase 2-induced endoplasmic reticulum stress. *Mol Med Rep* 16: 7205–7212, 2017. doi:10.3892/mmr.2017.7524.
55. **Park H, Go YM, St John PL, Maland MC, Lisanti MP, Abrahamson DR, Jo H.** Plasma membrane cholesterol is a key molecule in shear stress-dependent activation of extracellular signal-regulated kinase. *J Biol Chem* 273: 32304–32311, 1998. doi:10.1074/jbc.273.48.32304.
56. **Parmar KM, Larman HB, Dai G, Zhang Y, Wang ET, Moorthy SN, Kratz JR, Lin Z, Jain MK, Gimbrone MA Jr, García-Cardeña G.** Integration of flow-dependent endothelial phenotypes by Kruppel-like factor 2. *J Clin Invest* 116: 49–58, 2006. doi:10.1172/JCI24787.
57. **Pedersen NB, Wang S, Narimatsu Y, Yang Z, Halim A, Schjoldager KT, Madsen TD, Seidah NG, Bennett EP, Levery SB, Clausen H.** Low density lipoprotein receptor class A repeats are O-glycosylated in linker regions. *J Biol Chem* 289: 17312–17324, 2014. doi:10.1074/jbc.M113.545053.
58. **Peng M.** *Bioinformatics Applications in Proteomics Data Analysis* (PhD thesis). Utrecht, The Netherlands: Utrecht Univ., 2015.
59. **Sathanoori R, Rosi F, Gu BJ, Wiley JS, Müller CE, Olde B, Erlinge D.** Shear stress modulates endothelial KLF2 through activation of P2X4. *Purinergic Signal* 11: 139–153, 2015. doi:10.1007/s11302-014-9442-3.
60. **Seguchi T, Merkle RK, Ono M, Kuwano M, Cummings RD.** The dysfunctional LDL receptor in a monensin-resistant mutant of Chinese hamster ovary cells lacks selected O-linked oligosaccharides. *Arch Biochem Biophys* 284: 245–256, 1991. doi:10.1016/0003-9861(91)90292-Q.
61. **Simmons RD, Kumar S, Jo H.** The role of endothelial mechanosensitive genes in atherosclerosis and omics approaches. *Arch Biochem Biophys* 591: 111–131, 2016. doi:10.1016/j.abb.2015.11.005.
62. **Simons K, Ehehalt R.** Cholesterol, lipid rafts, and disease. *J Clin Invest* 110: 597–603, 2002. doi:10.1172/JCI0216390.
63. **Simons K, Gerl MJ.** Revitalizing membrane rafts: new tools and insights. *Nat Rev Mol Cell Biol* 11: 688–699, 2010. doi:10.1038/nrm2977.
64. **Soulis JV, Farmakis TM, Giannoglou GD, Louridas GE.** Wall shear stress in normal left coronary artery tree. *J Biomech* 39: 742–749, 2006. doi:10.1016/j.jbiomech.2004.12.026.
65. **Sprague EA, Steinbach BL, Nerem RM, Schwartz CJ.** Influence of a laminar steady-state fluid-imposed wall shear stress on the binding, internalization, and degradation of low-density lipoproteins by cultured arterial endothelium. *Circulation* 76: 648–656, 1987. doi:10.1161/01.CIR.76.3.648.
66. **Sun X, Fu Y, Gu M, Zhang L, Li D, Li H, Chien S, Shyy JY-J, Zhu Y.** Activation of integrin α5 mediated by flow requires its translocation to membrane lipid rafts in vascular endothelial cells. *Proc Natl Acad Sci USA* 113: 769–774, 2016. doi:10.1073/pnas.1524523113.
67. **Szmitko PE, Wang C-H, Weisel RD, de Almeida JR, Anderson TJ, Verma S.** New markers of inflammation and endothelial cell activation: Part I. *Circulation* 108: 1917–1923, 2003. doi:10.1161/01.CIR.0000089190.95415.9F.
68. **Tricot O, Mallat Z, Heymes C, Belmin J, Lesèche G, Tedgui A.** Relation between endothelial cell apoptosis and blood flow direction in human atherosclerotic plaques. *Circulation* 101: 2450–2453, 2000. doi:10.1161/01.CIR.101.21.2450.
69. **Tzima E, Irani-Tehrani M, Kiosses WB, Dejana E, Schultz DA, Engelhardt B, Cao G, DeLisser H, Schwartz MA.** A mechanosensory complex that mediates the endothelial cell response to fluid shear stress. *Nature* 437: 426–431, 2005. doi:10.1038/nature03952.
70. **Uzarski JS, Scott EW, McFetridge PS.** Adaptation of endothelial cells to physiologically-modeled, variable shear stress. *PLoS One* 8: e57004, 2013. doi:10.1371/journal.pone.0057004.
71. **Vizcaíno JA, Csordas A, del-Toro N, Dianes JA, Griss J, Lavidas I, Mayer G, Perez-Riverol Y, Reisinger F, Ternent T, Xu Q-W, Wang R, Hermjakob H.** 2016 update of the PRIDE database and its related tools. *Nucleic Acids Res* 44: D447–D456, 2016. doi:10.1093/nar/gkv1145.
72. **Wang T, Chen Z, Wang X, Shyy JY, Zhu Y.** Cholesterol loading increases the translocation of ATP synthase β chain into membrane caveolae in vascular endothelial cells. *Biochim Biophys Acta* 1761: 1182–1190, 2006. doi:10.1016/j.bbalip.2006.08.009.
73. **Wang Y, Flores L, Lu S, Miao H, Li YS, Chien S.** Shear stress regulates the Flk-1/Cbl/PI3K/NF-κB pathway via actin and tyrosine kinases. *Cell Mol Bioeng* 2: 341–350, 2009. doi:10.1007/s12195-009-0069-3.
74. **Warboys CM, Amini N, de Luca A, Evans PC.** The role of blood flow in determining the sites of atherosclerotic plaques. *F1000 Med Rep* 3: 5, 2011. doi:10.3410/M3-5.
75. **Xia J, Gill EE, Hancock RE.** NetworkAnalyst for statistical, visual and network-based meta-analysis of gene expression data. *Nat Protoc* 10: 823–844, 2015. doi:10.1038/nprot.2015.052.
76. **Xia J, Sinelnikov IV, Han B, Wishart DS.** MetaboAnalyst 3.0–making metabolomics more meaningful. *Nucleic Acids Res* 43: W251–W257, 2015. doi:10.1093/nar/gkv380.
77. **Yamamoto K, Ando J.** Vascular endothelial cell membranes differentiate between stretch and shear stress through transitions in their lipid phases. *Am J Physiol Heart Circ Physiol* 309: H1178–H1185, 2015. doi:10.1152/ajpheart.00241.2015.
78. **Yoshimura A, Yoshida T, Seguchi T, Waki M, Ono M, Kuwano M.** Low binding capacity and altered O-linked glycosylation of low density lipoprotein receptor in a monensin-resistant mutant of Chinese hamster ovary cells. *J Biol Chem* 262: 13299–13308, 1987.
79. **Zhou J, Lee PL, Lee CI, Wei SY, Lim SH, Lin TE, Chien S, Chiu JJ.** BMP receptor-integrin interaction mediates responses of vascular endothelial Smad1/5 and proliferation to disturbed flow. *J Thromb Haemost* 11: 741–755, 2013. doi:10.1111/jth.12159.